Monte Carlo simulation and theoretical calculation of SEM image intensity and its application in thickness measurement

Tian, Jinsen; Chiu, Yu-Lung; Wu, Jing

Link to publication on Research at Birmingham portal

Monte Carlo simulation and theoretical calculation of SEM image intensity and its application in thickness measurement

Jinsen Tian, Jing Wu, Yu-Lung Chiu[*]

School of Metallurgy and Materials, University of Birmingham, Edgbaston, Birmingham, B15 2TT, UK

Abstract

The intensity profiles of backscattered and secondary electrons from a pure Mg sample have shown a variation with sample thickness and acceleration voltage in the range of 5-30kV, depending on the specimen holder used. The intensities of backscattered electron (BSE) and secondary electron (SE) signals increases with the sample thickness until saturation when using a scanning transmission electron microscopy (STEM) holder with a closed tube below the sample. However the SE signal increases to the maximum and then decreases with the sample thickness when using a transmission Kikuchi diffraction (TKD) holder with no shielding below the sample whereas the BSE signal again increases until saturation. The influence of the holder on the SE signals is caused by the fact that secondary electrons emitted from the bottom surface could be detected only when using the TKD holder but not the STEM holder. The experimental results obtained are consistent with the Monte Carlo simulation results. Application of the magnitude of the SE and BSE signals to measurement of sample thickness have been considered and the BSE image profile shows a reasonably good accuracy.

Key Words: Monte Carlo simulation; secondary electron; backscattered electron; thickness measurement; SEM

1. Introduction

STEM-in-SEM reveals the internal structure of thin foil samples with high contrast and resolution due to the low voltage and thin sample utilized, which increase the electron scattering cross-sections and

---

[*] Corresponding author: Y.Chiu@bham.ac.uk (Yu-Lung Chiu)

reduce the interaction volume [1]. In the last few years, thin foil samples have also been widely used for diffraction study in SEMs. The so-called transmission Kikuchi diffraction (TKD) technique employs the traditional EBSD detectors but very thin samples [2]. Compared with bulk sample, it is more complicated for the SEM imaging of thin samples as the image contrast may vary with thickness, as well as composition and topography. So it is quite important to understand the expected contrast seen in both secondary electron (SE) and back-scattered electron (BSE) modes. A combination of Monte Carlo (MC) simulation and experiments help to interpret the image contrast and how it varies with imaging conditions, such as sample thicknesses and voltages.

On the other hand, it is important to obtain accurately the thickness of thin samples when the density of microstructure features, such as precipitates, dislocations and dispersoids is needed. It is also important for absorption and fluorescence effect corrections when energy dispersive spectroscopy (EDS) is used for composition analysis. Focused ion beam (FIB) can be used to cut the sample to reveal the cross section and then directly measure the sample thickness. However, this method is destructive. Electron energy loss spectroscopy (EELS) and convergent beam electron diffraction (CBED) have also been used widely to determine the sample thickness. For EELS, the thickness calculation is based on a simple relationship between the log-ratio intensity distribution and the ratio of mean free paths of electron inelastic scattering to sample thickness, that is $t = \lambda \ln(I/I_0)$, where t is the sample thickness, λ the mean free path of inelastic scattering, I the total intensity of the zero loss peak and the plasma peak and I_0 the intensity of the zero loss peak [3]. In the CBED [4], the sample thickness can be linked to the fringe minima observed as $\left(s_i^2 + \frac{1}{\xi_g^2}\right)t^2 = n_i^2$, where s_i is the deviation of the ith minimum from the exact Bragg position, ξ_g is the extinction distance and n_i an integer. Thickness can be determined from the slope of the plot of s_i^2 versus n_i^2. Both EELS and CBED methods can give a reliable thickness. Especially for CBED, in which case the relative error is better than 2-5% even with the above simple version of the formula[5]. Even better accuracy can be obtained by quantitative many-parameter fits to the intensity profiles of the CBED discs[6]. However, both methods are time consuming, especially when many thickness measurements are needed.

Since the BSE coefficient and SE yield have been widely researched using experiments and theoretical calculations and for thin samples, both depend on the thickness [7]. There is a potentially more efficient way to determine the thickness of a specimen based on the BSE coefficient and SE yield obtained. In this paper, the intensity profiles of both BSE and SE images were measured experimentally vis-à-vis Monte Carlo (MC) simulations and theoretical calculations, and the application to thickness determination is discussed.

2. Experimental procedure and simulation

Pure Mg TEM samples of 3 mm diameter were prepared by twin-jet polishing using a solution containing lithium chloride 8.8 g, magnesium perchlorate 19.3 g, methanol 833 mL and butoxyethanol 167 mL, at a voltage of 70 V and a temperature of -45 ºC. Both BSE and SE images were taken at different acceleration voltages (HV) of 5, 10, 15, 20, 25 and 30 kV using two different sample holders (an STEM holder and a TKD holder) in a TESCAN Mira microscope (the configurations are shown in Figure 1). The SE and BSE detectors used are an Everhart Thornley detector with standard grid bias and a YAG detector with a single annular scintillator, respectively. The other imaging conditions were kept the same. The image intensity profiles versus distance from the edge of the hole were obtained from defined positions. The sample was finally cut apart using the FIB at these defined locations to directly measure the thickness of the sample.
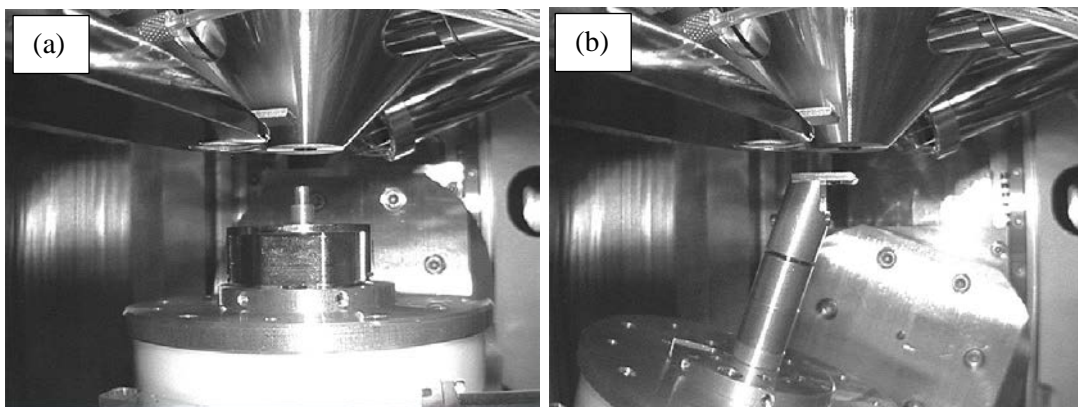

Fig.1 two types of holders used in this study: (a) STEM holder and (b) TKD holder

MC simulation of the SE and BSE yields was done using CASINO version 3.3 [8] with a thickness step of 0.1 μm from 0.1 μm to a thickness when no electrons can get through the sample and with

different energies from 5 to 30 keV in steps of 5 keV. At 5 keV, the initial thickness was set as 10 nm with a step size of 10 nm. In every case, 1,000,000 electrons were considered. The cut-off energy was set to 50 eV for all the conditions. It has been shown that the mean penetration depth in aluminium is less than 1 Å when the cut-off energy changed from 100 eV to 20 eV [9]. So the effect of cut-off energy used in the current work on the SE and BSE signals and therefore the thickness determination was regarded as negligible. The modified Bethe formula given by Joy and Luo[10] and Lowney [11] was used to determine the stopping power and the scattering cross section was calculated by ELSEPA model [12].

The BSE coefficient of bulk samples has been widely researched using both experiment and theoretical calculation as it is the foundation of the BSE imaging. Hunger[13] measured the BSE coefficients of 28 elements and derived an analytical expressions of the dependence of BSE coefficient on the electron energy and the atomic number. For light elements with Z smaller than about 50, the BSE coefficient decreased with increasing incident electron energy and vice versa. However Everhart [14] derived a formula which showed that the BSE coefficient was independent of the incident electron energy, which is consistent with the MC simulations using both single and plural scattering models. Joy [7] suggested the inconsistences between the experimental results [13] and computed data [14] probably arose from the variety of methods used to measure the BSE coefficient. Compared with bulk samples, BSE coefficients of thin samples have received little attention with regard to the relationship between BSE coefficients and thickness. Niedrig[15] reported a linear relationship between BSE efficiency and the sample thickness for most elements (except those with low atomic number) in the low thickness region which is much smaller than the penetration depth of the incident electrons, and proposed a model to interpret the experimental results. Nakhodkin[16] extended the Everhart model to films with thicknesses between 0 and R/2, where R is the maximum penetration depth. Using a simple potential between electron and atom, Kanaya [17] (please confirm this) obtained an equation which can be used to calculate the BSE coefficient over the whole range 0 to R, the predicted BSE coefficients were much bigger than the experimental results[18]. MC

simulation has therefore been carried out to determine the dependence of BSE coefficient on the thickness.

In contrast to BSE coefficients, SE yields do not depend upon the atomic number, while strongly depend on the incident electron energy [19]. Baroody [20] formulated a theory based on the Sommerfeld model [21] and pointed out that the dependence of SE yield on incident electron energy can be described using a single curve. However, the calculated data were lower than the experimental results [20]. After that, several theories were proposed to calculate the SE yield, e.g. by Seiler [22], Dionner [23]. Joy [24] thoroughly examined the correlation between SE yields (δ) and the primary electron energy (E_{PE}) for 44 elements and proposed a semi-empirical law to describe the correlation

$$\frac{\delta}{\delta^m} = 1.28(\frac{E_{PE}}{E_{PE}^m})^{-0.67}\left\{1 - \exp[-1.614(\frac{E_{PE}}{E_{PE}^m})^{1.67}]\right\}$$

where δ^m is the maximum SE yield and E_{PE}^m the corresponding energy for the maximum SE emission. For Mg, the parameters were set as 0.8 and 240 eV respectively, which agree reasonably well with the experimental results of 0.8 and 300 eV and the calculated results of 0.67 and 280 eV by Kanaya [25]. Only those SE excited near the surface can reach the surface and escape from it. The escape depth had been revealed by MC simulation, indicating that the escape depth in Cr for 20 keV electrons was about 3 nm[26]. This is consistent with the result of Seiler [22], which showed that the escape depth of SE is about 5λ where λ is the mean free path of SE and of the order of 5 nm and 75 nm for metals and insulators, respectively. This can be used to explain why the SE intensity profiles had a step at the edge of the holes. As the sample thickness is much greater than 5 nm, the SE yields by PE saturated immediately even at the edge.

Considering the contribution of BSE, the total SE yields from the top surface of a thin sample can be derived as

$$\delta = \delta_{PE}(1 + \beta\eta)$$

where δ_{PE} is SE yield by primary electrons (PE), β is the ratio of the SE generated by a BSE and by a PE, and η the BSE coefficient. BSE energy is smaller than the PE energy but larger than E_{PE}^m (240 eV for Mg) and within this energy range, the SE yields increased with decreasing incident electron

energy [24]. Also, the BSE had a broad angular distribution and Kanter's experiment [27] showed that the SE yields increased with the tilt angle when the incident electron energy was above 5 keV. Both of the above factors indicated that β should be larger than unity 1. This was confirmed by experiments and MC simulations [28-30]. Reimer's results indicated β is in the range of 1.5 - 3 for both Al and Au with the incident electron energy in the range of 10 – 35 keV [28]. This is smaller than the MC simulation predicted value of 2 – 5 [29] and Drescher's [30] experimental results of 4 - 6. As the BSE energy and angular distribution depend on the thickness of the sample, β also should be related to the thickness and can be described by a distribution function f (E, θ). However, an accurate expression of f(E, θ) is not available. As a simplification, f(E, θ) can be estimated as $f_1(E)*f_2(\theta)$, i.e. β can be calculated by considering the contributions of energy and angular distribution separately. The contribution of energy distribution has been discussed by Joy [24], while the contribution of angular broadening can be calculated by [28]

$$\beta_\theta = \frac{\int_0^{\pi/2} f_2(\theta) \sec\theta \sin\theta d\theta}{\int_0^{\pi/2} f_2(\theta)\sin\theta d\theta}$$

Both the energy and angular distribution can be obtained by MC simulation. In this work, the SE yield excited by PE was calculated and the BSE coefficient derived from MC simulation. The calculated results were compared with the MC simulation.

As MC simulation did not provide the SE yield from both surfaces, calculations were conducted. To calculate the SE yield from the bottom surface, we started with the calculation of the maximum range (R) the electrons can get through and the transmission possibility in Mg. The transmitted electron energy and the exit angle from the bottom surface will also be considered to calculate the SE yield caused by the transmitted electrons. The maximum range of electron can be calculated by the integration of dE/ds, the stopping power proposed by Bethe [31] as

$$\frac{dE}{ds} = -78500 \frac{\rho Z}{AE} \ln(\frac{1.166E}{J})$$

where Z is the atomic number, ρ the density of material, A the atomic weight and J the mean ionization potential. Based on experimental measurements, Burger [32] proposed the dependence of J on Z as

$$J = \left(9.76Z + \frac{58.5}{Z^{0.19}}\right) \cdot 10^{-3}$$

For Mg, J was determined to be 154 eV.

This model is consistent with the results of Tung [33] calculated based on a statistical model when E is larger than 1 keV, while it gives a much smaller prediction in the lower energy range because J is energy dependent rather than a constant. Joy [10] modified Bethe's model to incorporate this energy dependence by adding a correction term:

$$\frac{dE}{ds} = -78500 \frac{\rho Z}{AE} \ln\left[\frac{1.166(E + 0.85J)}{J}\right]$$

The modified model is consistent with Bethe's model in the high energy range, and the accuracy was improved in the low energy range. According to XXX (reference), a residual term of 0.4 eV/nm showed the best fit with experimental results. The same residual term was used in the present simulation using CASINO v3.3. The maximum range of the electrons can then be calculated by the integration of the stopping power. In this paper, R was determined to be 0.50, 1.6, 3.2, 5.2, 7.6 and 10.3 μm for HV used at 5, 10, 15, 20, 25 and 30 kV, respectively.

The transmission possibility calculated by Kanaya's semi-empirical formula was smaller for elements of low atomic number in the range of 0-0.3R due to the overestimation of the scattering cross section[17]. Fitting [34] also formulated a normalized formula to describe the experimental data

$$\eta_T = \exp\left[-4.605 \left(\frac{x}{R}\right)^p\right]$$

where p is a transmission parameter which reflected the different efficiency ratios of elastic and inelastic processes in different target materials and dependent on the atomic number and the initial electron energy. Experimental results [35] indicated that p is about 2 for Al and 2.2 for Si in the

energy range of 5-30 keV and can be written for a wide range of atomic number and energy (3<Z<80, 1 keV < E < 1 MeV) as

$$p = (0.8 + 2B_0)\ln(\frac{1}{B_0})$$

where B_0 is the backscattering coefficient. According to this relationship, p was determined as 2.2 for all the energy ranges used in the current work.

The electron energy after getting through the material can be calculated by integration of the stopping power. However, this overestimates the energy as the beam broadening has not been taken into consideration.

Similar to SE excited by BSE, the energy and angular distribution should be taken into consideration when calculating the SE yields from the bottom surface. The energy distribution can be obtained by MC simulation. However, the angular distribution is not provided by MC simulation. As a simplification, the most probable angle of the transmitted electron was used. Cosslett's experiments [36] indicated that the most probable angle increases with increasing sample thickness as

$$\lambda_A^2 = 1.2 \times 10^7 \frac{Z^{3/2}}{E_0} \frac{\rho x}{A}$$

where λ_A is the most probable angle and the other parameters as defined earlier.

The total SE yields can then be obtained as the sum of the SE excited by primary electrons, BSEs and transmitted electrons.

3. Results and Discussions

The experimental SE and BSE images and the corresponding image intensity profiles obtained using *Image-Pro Plus* versus the sample thickness using different holders and HVs are shown in figure 2 and figure 3. The red line in figure 3 shows the position where intensity profile was obtained. Noticeably strong SE signals were detected in the hole with TKD holder but not with the STEM holder. This is probably due to the interaction between electrons and the stage underneath the

It can be seen from figure 3 that the intensity profiles of the BSE images were quite similar for both holders, increasing with thickness until saturation. However, the trends were different with different holders for the SE image intensity. Using the STEM holder, the SE image intensity profile increased with the thickness until saturation, which is similar to the BSE profiles though the SE profiles had a step at the edge of the hole. With the TKD holder, the intensity increased to a maximum value and then decreased.
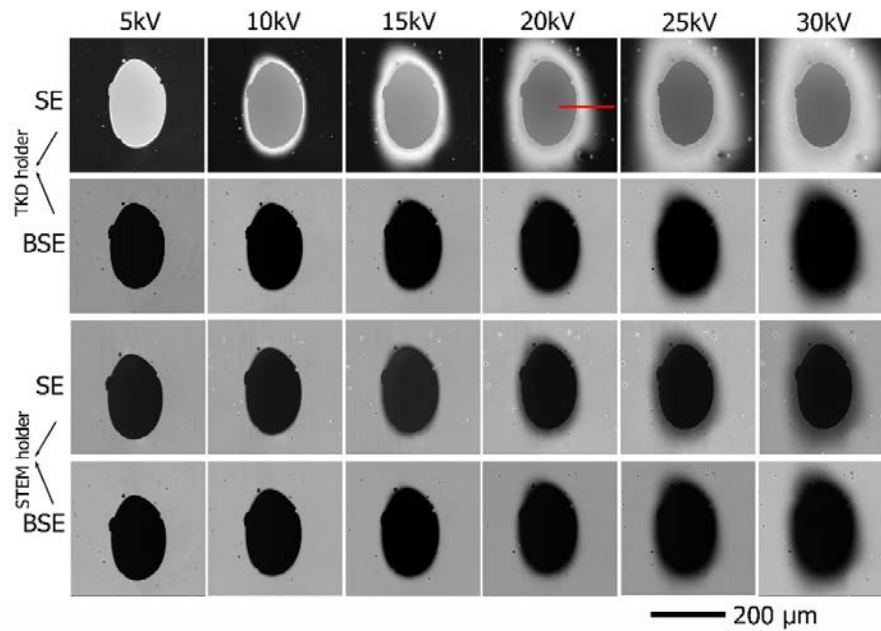

Fig.2 BSE and SE images obtained under different HVs with holders. Red line shows the position where intensity profile was obtained.
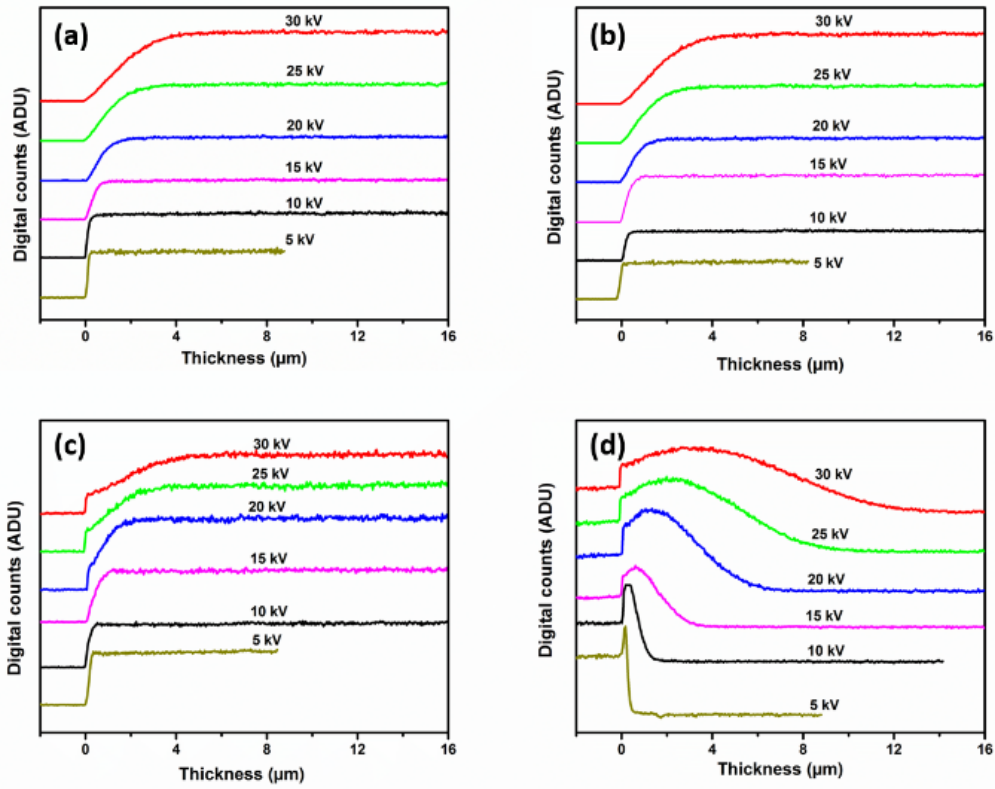
Fig.3 Intensity profiles versus thickness extracted from: (a) BSE image with STEM holder, (b) BSE image with TKD holder, (c) SE image with STEM holder and (d) SE image with TKD holder
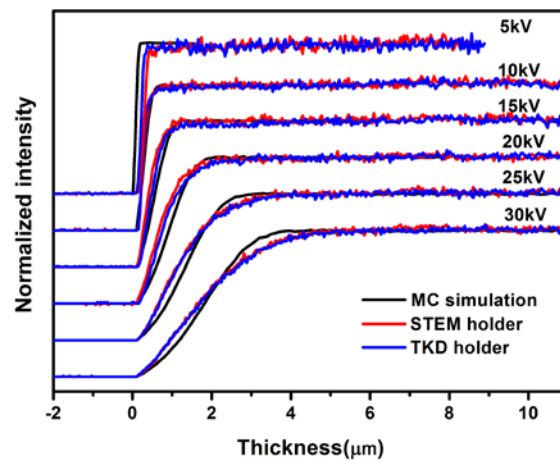
3.1 BSE intensity

Fig.4 Comparison of normalized BSE intensity profiles between simulation and experiments

The BSE yields in the MC simulation and experiments are illustrated in figure 4. To make a direct comparison, the profiles were normalized by setting the minimum and maximum as 0 and 1 respectively. From figure 4 it can be seen the simulated curve is consistent with the experimental curve, increasing with thickness to a saturation value. The thickness when the BSE reached to saturation can be obtained from the simulation (experimental) curves as 0.18 (0.38), 0.7 (0.82), 1.2 (1.34), 2.0 (2.27), 3.0 (3.53) and 3.9 µm (4.51 µm) with an HV of 5, 10, 15, 20, 25 and 30 kV, respectively. The simulated value is lower than that of the experimental results. Residual terms of smaller values than 0.4 eV/nm have been assessed which obviously generated slightly larger thickness calculated. However the material dependence of the residual term needs to be defined as future work.

3.2 SE yields

The resultant SE yields from the top surface are shown in figure 5. Similar to BSE, the image intensity profiles were normalized. The trend that SE yields increased with thickness until saturation is consistent with the SE image intensity profiles obtained. There is a sudden change of the intensity profile between hole and sample, resulting in the formation of a step. The point when the intensity profile deviated at the step was determined and set as the zero point. The experimental results and MC simulated results agree reasonably well except that the thickness when SE yields reach to saturation for simulation and calculation is lower than experimental results. This is reasonable as it has been shown that the increasing SE yields are due to the increasing BSE yields and the saturation thickness for BSE curve is lower by simulation than experiment.

When using the STEM holder, only electrons excited from the top surface were collected by the detector as electrons exited from the bottom surface were confined within the tube of the holder. However, the TKD holder offers no shielding of the electrons exited from the bottom surface. With the bias of the SE detector, those SE exited from the bottom surface can also be detected, thus resulted in different SE image intensity profiles compared with those used the STEM holder.
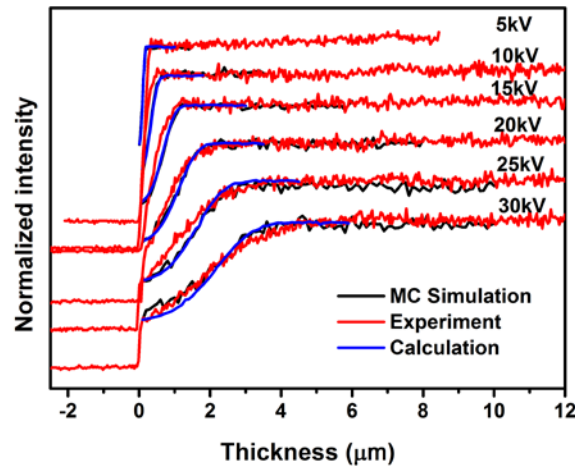
Fig.5 Comparison of normalized SE intensity in the top surface between simulation, experiments and calculation.

The normalized result is shown in figure 6. With increasing sample thickness, the SE yield increases to a maximum value and then decreases. The total SE yields can be divided into three parts, i. e. the contribution from the PE, BSE, and the transmission electrons. SE generated by PE is a constant. Contributions from BSE increased until saturation. SE yields from the bottom surface decrease to 0 as the transmission possibility decreases. The sum of these three parts results in a peak. Also, with increasing incident electron energy, the peak shifted towards larger thickness side. This is consistent with experimental results. To compare quantitatively the result of MC simulation and that of the experiment measurement, the image intensity profiles were normalized and are shown in figure 6. It can be seen that there were deviations between the experimental and the simulation results though the trends of the intensity profiles are consistent. There are two characteristic thicknesses, one is the peak thickness, and the other is the saturation thickness. The peak thickness for calculation (experiment) is determined to be 0.08 (0.17), 0.2 (0.25), 0.6 (0.61), 0.9 (1.06), 2.3 (2.58) and 2.7μm (3.22μm), for 5, 10, 15, 20, 25 and 30kV, respectively. The simplification of the contribution of angular distribution used and the neglect of collection efficiency may contributed to the difference between the simulation and the experimental results observed. The saturation thickness is 0.5 (0.61), 1.6 (1.74), 3.2 (3.68), 5.2 (6.85), 7.6 (10.32) and 10.3μm (13.86μm) for simulation (experiment) and for 5, 10, 15, 20, 25 and 30kV. This difference is due to the penetration depth which is determined by stopping power which
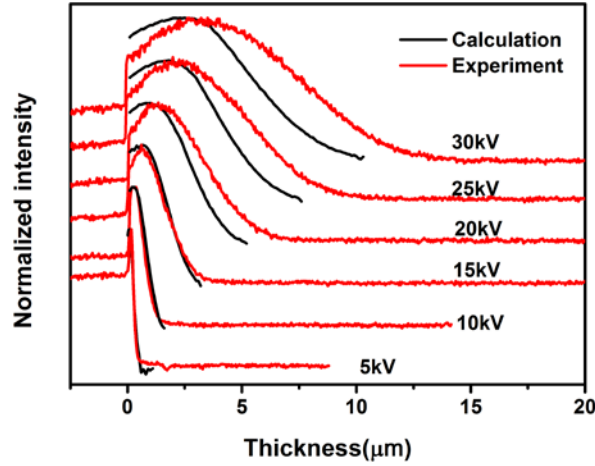
12

Fig.6 Comparison of normalized total SE yield between the calculation and the experiments.

3.3 Application to thickness determination

As discussed in the above section, the SEM image intensity is related to sample thickness and thus in principle can be used to measure thin foil sample thickness. Figure 4 indicated that BSE image intensity profiles with different holders were identical while the SE image intensity profiles vary depending on the holder used. Also, for SE image, more factors had to be taken into consideration because SE can be generated by primary electrons, BSEs and transmitted electrons and the collection efficiency might be different for SE yielded at the top and bottom surfaces. Moreover, it has been stated that to normalize or fit the intensity profiles of SE image obtained using the STEM holder, the height of the steps due to the sudden change of the intensity had to be determined, which could not be done precisely. For the SE images obtained using the TKD holder, it is difficult to find accurate mathematical expressions to calculate the SE yield. On the other hand, the electron backscattering process is less sensitive to the surface condition and surface texture than the SE emission. As such the BSE image intensity profiles are more reliable for the sample thickness determination. Experimental profiles can be used as references to determine sample thickness by comparing the intensity profiles

with that of samples whose thickness were unknown. A four-parameter (t_0, A_1, A_2, A_3) sigmoidal curve

$$\eta = A_2 + \frac{A_1 - A_2}{1 + \exp(\frac{t - t_0}{A_3})}$$

has been shown to provide the best description of the experimental BSE intensity profile [37]. Using the same equation, a normalized experimental intensity profile of the BSE image with the incident electron energy of 30 kV using the STEM holder is shown in figure 7(a), together with a fitting curve using the same equation above. The parameters used are also shown in figure 7(a). Similar results could be obtained for other incident electron energies. By using this profile as a reference, the thickness of other samples with same composition can be directly derived by measuring the normalized intensity profile. An example was shown in figure 7(b) where the thickness derived using the above method is compared with the thickness measured from a FIB prepared sample. The difference between the two is less than 10%. Compared with other thickness measurement techniques like CBED and EELS, this method is much more efficient as only a BSE image is required. This could be useful when the sample thickness at various positions needs to be determined repeatedly on different samples of the same material composition.
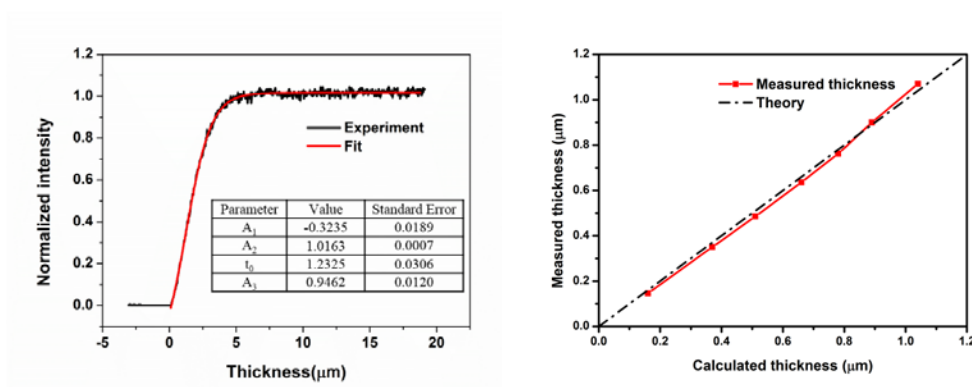

Fig.7 (a) Normalized experimental and fitted curves with HV of 30kV and STEM holder with fitted parameters embedded, (b) comparison of the measured and calculated thickness

4. Conclusion

Both the BSE image and SE image intensity profiles obtained from samples of different thicknesses and incident electron energies were studied using MC simulation and analytical calculation using either the STEM holder or the TKD holder. The results obtained agree reasonably well with the experimental obtained image intensity profiles. The BSE image intensity profile can be used to determine the sample thickness with a reasonably good accuracy.

References

1.	Merli, P.G. and V. Morandi, *Low-Energy STEM of Multilayers and Dopant Profiles.* Microscopy and Microanalysis, 2005. **11**(1): p. 97-104.
2.	Trimby, P.W., *Orientation mapping of nanostructured materials using transmission Kikuchi diffraction in the scanning electron microscope.* Ultramicroscopy, 2012. **120**: p. 16-24.
3.	Egerton, R.F., *Electron Energy Loss Spectroscopy in the Transmission Electron Microscope.* 1986, New York: Plenum Press.
4.	Mac Gillavry, v.C.H., *Zur prüfung der dynamischen theorie der elektronenbeugung am kristallgitter.* Physica, 1940. **7**(4): p. 329-343.
5.	Allen, S.M. and E.L. Hall, *Foil thickness measurements from convergent-beam diffraction patterns An experimental assessment of errors.* Philosophical Magazine A, 1982. **46**(2): p. 243-253.
6.	Spence, J.C.H. and J.M. Zuo, *Electron microdiffraction.* 1992: Plenum Press.
7.	Joy, D.C., *Monte Carlo Modeling for Electron Microscopy and Microanalysis"(Oxford Series in Optical and Imaging Sciences).* 1995.
8.	Demers, H., et al., *Three-Dimensional Electron Microscopy Simulation with the CASINO Monte Carlo Software.* Microscopy and Microanalysis, 2017. **17**(S2): p. 612-613.
9.	Valkealahti, S. and R.M. Nieminen, *Monte-Carlo calculations of keV electron and positron slowing down in solids.* Applied Physics A, 1983. **32**(2): p. 95-106.
10.	Joy, D.C. and S. Luo, *An empirical stopping power relationship for low-energy electrons.* Scanning, 1989. **11**(4): p. 176-180.
11.	Lowney, J.R., *MONSEL-II - MONTE-CARLO SIMULATION OF SEM SIGNALS FOR LINEWIDTH METROLOGY.* Microbeam analysis, 1995. **4**(3): p. 131-136.
12.	Salvat, F., A. Jablonski, and C.J. Powell, *elsepa—Dirac partial-wave calculation of elastic scattering of electrons and positrons by atoms, positive ions and molecules.* Computer Physics Communications, 2005. **165**(2): p. 157-190.
13.	Hunger, H.J. and L. Küchler, *Measurements of the electron backscattering coefficient for quantitative EPMA in the energy range of 4 to 40 keV.* physica status solidi (a), 1979. **56**(1): p. K45-K48.
14.	Everhart, T.E., *Simple Theory Concerning the Reflection of Electrons from Solids.* Journal of Applied Physics, 1960. **31**(8): p. 1483-1490.
15.	Niedrig, H., *Electron backscattering from thin films.* Journal of Applied Physics, 1982. **53**(4): p. R15-R49.
16.	Nakhodkin, N.G., A.A. Ostroukhov, and V.A. Romanovskii, *ELECTRON INELASTIC SCATTERING IN THIN FILMS.* Journal Name: Soviet Phys.-Solid State (English Transl.); Journal Volume: Vol: 4; Other Information: Orig. Receipt Date: 31-DEC-63, 1962: p. Medium: X; Size: Pages: 1112-19.
17.	Kanaya, K. and S. Okayama, *Penetration and energy-loss theory of electrons in solid targets.* Journal of Physics D: Applied Physics, 1972. **5**(1): p. 43.
18.	Joy, D.C., *A database on electron-solid interactions.* Scanning, 1995. **17**(5): p. 270-275.

19.   Joy, D.C., *Monte Carlo Modeling for Electron Microscopy and Microanalysis*. 1995: Oxford University Press.

20.   Baroody, E.M., *A Theory of Secondary Electron Emission from Metals.* Physical Review, 1950. **78**(6): p. 780-787.

21.   Sommerfeld, A., *Zur Elektronentheorie der Metalle auf Grund der Fermischen Statistik.* Zeitschrift für Physik, 1928. **47**(1): p. 1-32.

22.   Seiler, H., *Secondary electron emission in the scanning electron microscope.* Journal of Applied Physics, 1983. **54**(11): p. R1-R18.

23.   Dionne, G.F., *Origin of secondary‐electron‐emission yield‐curve parameters.* Journal of Applied Physics, 1975. **46**(8): p. 3347-3351.

24.   Lin, Y. and D.C. Joy, *A new examination of secondary electron yield data.* Surface and Interface Analysis, 2005. **37**(11): p. 895-900.

25.   Kawakatsu, K.K.a.H., *Secondary electron emission due to primary and backscattered electrons.* J. Phys. D: Appl. Phys, 1972.

26.   Joy, D.C., in *Microbeam Analysis*, A.R.a. J.I. and R.J. Goldstein, Editors. 1984, San Francisco Press: Pennsylvania. p. 81.

27.   Kanter, H., *Contribution of Backscattered Electrons to Secondary Electron Formation.* Physical Review, 1961. **121**(3): p. 681-684.

28.   Reimer, L. and H. Drescher, *Secondary electron emission of 10-100 keV electrons from transparent films of Al and Au.* Journal of Physics D: Applied Physics, 1977. **10**(5): p. 805.

29.   Shimizu, R., *Secondary electron yield with primary electron beam of kilo‐electron‐volts.* Journal of Applied Physics, 1974. **45**(5): p. 2107-2111.

30.   H. Drescher, L. Reimer, and H. Seidel, Z. Angew. Phys., 1970. **29**: p. 331-336.

31.   Bethe, H., *Zur Theorie des Durchgangs schneller Korpuskularstrahlen durch Materie.* Annalen der Physik, 1930. **397**(3): p. 325-400.

32.   Science, N.R.C.C.o.N., *Studies in Penetration of Charged Particles in Matter*. 1964: National Academy of Sciences-National Research Council.

33.   Tung, C.J., J.C. Ashley, and R.H. Ritchie, *Electron inelastic mean free paths and energy losses in solids II: Electron gas statistical model.* Surface Science, 1979. **81**(2): p. 427-439.

34.   Fitting, H.J., *Transmission, energy distribution, and SE excitation of fast electrons in thin solid films.* physica status solidi (a), 1974. **26**(2): p. 525-535.

35.   F, M.A., Sov. Phys.-Solid State, 1960. **2**: p. 1934-1951.

36.   Thomas, V.E.C.a.R.N., *Multiple scattering of 5-30 keV electrons in evaporated metal films: I. Total transmission and angular distribution.* Br. J. Appl. Phys. , 1964.

37.   Haimovich, J., K. Leibold, and G. Staudt, *Estimating and Measuring Thickness of Thin Layers by Monte Carlo Simulation and Backscattered Electron Image Analysis.* AMP Journal of Technology, 1996. **5**: p. 65-78.